Chemistry and aerosols in the marine boundary layer: 1-D modelling of the three ACE-2 Lagrangian experiments

Karsten Suhre[a], Vincent Crassier[a,*], Céline Mari[a], Robert Rosset[a], Doug W. Johnson[b], Simon Osborne[b], Robert Wood[b], Meinrat O. Andreae[c], Brian Bandy[d], Timothy S. Bates[e], Steven Businger[f], Christian Gerbig[g], Frank Raes[h], Jochen Rudolph[i]

Abstract

Three Lagrangian experiments were conducted during IGAC's second aerosol characterization experiment (ACE-2) in the area between Portugal, Tenerife and Madeira in June/July 1997. During each Lagrangian experiment, a boundary layer air mass was followed for about 30 h, and the temporal evolution of its chemical and aerosol composition was documented by a series of vertical profiles and horizontal box pattern flown by the Meteorological Research Flight research aircraft Hercules C130. The wealth of observational data that has been collected during these three Lagrangian experiments is the basis for the development and testing of a one-dimensional Lagrangian boundary layer model with coupled gas, aqueous, and aerosol phase chemistry. The focus of this paper is on current model limitations and strengths. We show that the model is able to represent the dynamical and chemical evolution of the marine boundary layer, in some cases requiring adjustments of the subsidence velocity and of the surface heat fluxes. Entrainment of a layer rich in ozone and carbon monoxide from a residual continental boundary layer into the marine boundary layer as well as in-cloud oxidation of sulphur dioxide by hydrogen peroxide are simulated, and coherent results are obtained, concerning the evolution of the small, presumably sulphate–ammonia aerosol mode.

Keywords: Aerosol; Marine boundary layer; Lagrangian

1. Introduction

The second aerosol characterization experiment (ACE-2) of the International Global Atmospheric Chemistry (IGAC) programme was conducted from 15 June to 31 July 1997 over the Atlantic Ocean in the area between Portugal, Maderia and Tenerife (Raes et al., 2000 and references therein). During this period, this area was affected several times by European outbreaks of air that occur frequently during the summer months when the Azores high-pressure system moves eastward over the European continent. With the objective to study the aging of the chemical and aerosol composition of these air masses, such as ozone, carbon monoxide, sulphur

dioxide, hydrogen peroxide, different volatile organic compounds, and aerosol characteristics, three Lagrangian experiments were conducted during ACE-2. (Johnson et al., 2000a). In each of these experiments, a boundary layer air mass was "tagged" by the release of one or several "smart" balloons (Businger et al., 1996, 1999) drifting with the wind at about 500 m altitude in the marine boundary layer. The chemical and aerosol composition of each "tagged" air mass was then documented for a period of about 30 h through three successive flights of the meteorological research flight (MRF) research aircraft Hercules C130 by a series of vertical profiles and horizontal box pattern (Johnson et al., 2000a).

Each of the three ACE-2 Lagrangian experiment has its particularity: the first one took place in an unpolluted maritime air mass, whereas the second and the third sampled polluted European continental air and its aging over the ocean. The second Lagrangian was completely overcast, while the first and third Lagrangian encountered only fractional cloud cover. The air sampled during the second Lagrangian was freshly polluted and left the continent not more than 12 h before the release of the balloons, while the air of the third Lagrangian was already over the ocean for at least two days. All three Lagrangian experiments took place under anticyclonic conditions in a southbound airflow directed over warmer water. Under the combined effect of the resulting subsidence and boundary layer growth, the residual continental boundary layer (RCBL), that overlaid the marine boundary layer (MBL) in both polluted Lagrangians, was gradually entrained into the growing MBL throughout the experiment. A detailed description of the meteorological conditions and the chemical and aerosol observations of each of the three experiments are given by Johnson et al. (2000b), Osborne et al. (2000), and Wood et al. (2000), respectively. The aerosol chemical composition for all three Lagrangians is discussed by Andreae et al. (2000), and the mesoscale meteorological situation is described by Suhre et al. (2000).

In an ideal setting, the Lagrangian approach allows the investigators to eliminate the advective contribution from the budget equation of any observed variable, such as the concentration of aerosol number and mass or that of a reactive chemical species in the atmospheric boundary layer (Huebert et al., 1996). The remaining unknowns in this box model approach that need to be determined are then the deposition or emission fluxes at the surface and the entrainment fluxes across the boundary layer top. In the "real world", however, the marine boundary layer rarely behaves like an idealized well-mixed box, but rather like a one-dimensional vertically differentiated column (Suhre et al., 1995; Bretherton and Pincus, 1995; Russel et al., 1998; Suhre et al., 1998, S98 hereafter; Wang et al., 2000). Therefore, a one-dimensional (1-D) meteorological boundary layer model with coupled chemistry allows a much more comprehensive approach in the interpretation of a Lagrangian experiment than does a zero-dimensional box-model. Processes such as cloud cycling entrainment of free tropospheric air into the MBL, and turbulent exchange between the layers with different thermal stratification can be represented with much more detail and physical realism. The presence of clouds, for instance, is usually simulated in a box model by assuming a certain frequency of cloud occurrence and by switching the presence of cloud water on and off (Raes, 1995), whereas in a 1-D boundary layer model, cloudy and non-cloudy layers may coexist and turbulent exchange between them is parameterized based on physical principles (Bougeault and Lacarrère, 1989). Also, in a 1-D model, the cloud water vertical profile is not imposed but may evolve in time as simulated by the model. Another example is the entrainment flux: in a box model, this flux has to be given as an external forcing parameter, whereas in a 1-D model boundary layer growth, and thus entrainment, is simulated prognostically, depending on wind shear, large-scale subsidence and surface heat fluxes. As a last example, consider a boundary layer with a more complicated vertical layered structure, such as a radiatively decoupled case that occurs frequently in the Azores region (e.g. Suhre and Rosset, 1994). Although a box model still can be adapted to such a situation by assuming several boxes that are interconnected by inter-box exchange fluxes, the uncertainties in the results of such a model increases strongly with the number of forcing parameters that have to be introduced. Finally, with respect to initialization and validation, a 1-D Lagrangian modelling approach is also ideally adapted to the analysis of Lagrangian experiments (as long as vertical shear remains weak). The first aircraft sounding allows a full initialization of all observed variables, and all successive aircraft soundings can be compared on a one-to-one basis with profiles from the 1-D simulation at the corresponding model time.

This brings us to the objectives of this work. Integrative numerical modelling of coupled dynamical and chemical systems typically serves two goals. One is the assessment of our current understanding of complex systems; here the aging of a polluted air mass over the ocean. The other is the development of a modelling tool that will eventually allow the assessment of the larger three-dimensional picture of regional and continental pollutant transport and transformation, aimed at air pollution evaluation and political decision making. We claim that if we validate the 1-D model for a number of representative situations spanning the full range of conditions (pollutant composition, concentration and size distribution, boundary layer type, cloud type, subsidence rate, etc.), and if we then validate the advection part of the model in its three-dimensional (3-D) configuration independently, using for example, passive tracer experiments such as the European tracer experiment (ETEX) (Van Dop et al.,

1998), then we have validated the model as a whole, provided the 1-D model implements exactly the same parameterizations as what is implemented in the 3-D mesoscale model (Lafore et al., 1998). In this context, the present work should also be understood as the logical continuation of the earlier work of S98 on the unpolluted, shear-driven boundary layers that were observed during ACE-1.

The questions we will address in this paper are then: How well does the 1-D model simulate?

- the vertical boundary layer structure and its evolution,
- the turbulent mixing and entrainment of major trace gases,
- their gas- and liquid-phase chemical transformations, and
- the evolution of the aerosol composition and size distribution.

Moreover, this work will also allow us to stress out and try to explain the reasons for differences between our model and observations.

2. Model description

The model used here is the new French mesoscale meteorological model Méso-NH (Lafore et al., 1998) in its one-dimensional Lagrangian configuration. It has been previously described in Suhre et al. (1998). The dynamical part of the model consists of what is commonly called a 1-D boundary layer model. It has a prognostic equation for turbulent kinetic energy (Redelsperger and Sommeria, 1981; Stull, 1988) with a nonlocal mixing length scheme (Bougeault and Lacarrère, 1989) and it uses the classical Kessler (1969) bulk warm cloud microphysical parameterization for the prediction of water vapor, cloud water and rain variables. A partial cloudiness scheme (Bechtold et al., 1992) is used to represent fractional cloud cover in grid cells that are close to saturation, and visible and infrared radiative heating and cooling processes are implemented following Morcrette (1989) and Morcrette and Fouquart (1985). Surface momentum and heat fluxes over the ocean are based on Charnock's Charnock (1955) parameterization, with the sea-surface temperature evolving after meteorological analyses. Large-scale subsidence is imposed as a vertical advection forcing with a zero-gradient upper boundary conditions. Large-scale pressure gradient forcing is modelled using a geostrophic wind. A fixed vertical grid spacing of 25 m is applied up to 1000 m altitude and is then gradually increased by 6% per grid point up to the model top at about 2850 m, yielding a total of 70 vertical levels.

A number of new developments have been introduced in the chemistry module since the S98 work. The gas-phase reaction scheme has been extended to the "regional atmospheric chemistry mechanism" (RACM) (Stockwell et al., 1997) that treats 77 chemical species with 237 reactions. Photolysis rates are calculated on-line and in interaction with the modelled cloud cover, using the tropospheric ultraviolet visible (TUV) model, version 3.9 (Madronich and Flocke, 1998). Dry deposition is parameterized using a multiple resistance approach (Seinfeld and Pandis, 1998 and references therein), the aerodynamic resistance being taken from the mesoscale model's surface scheme. Aqueous-phase chemistry is included by calculating the equilibrium between the gas- and the liquid-phase concentrations of CO_2, H_2SO_4, SO_2, HNO_3, H_2O_2, NH_3, O_3 and their respective ions (Seinfeld and Pandis, 1998), based on the modelled cloud water content at each model level. A fixed NH_3 mixing ratio of 500 ppt (based on measurements at Tenerife) and a CO_2 mixing ratio of 330 ppm are assumed in the equilibrium calculations. The oxidation of SO_2 by O_3 and H_2O_2 in the cloud phase as a function of the resulting cloud–water pH and resolved reactant concentrations is then taken into account through the implementation of equivalent reactions in the gas-phase mechanism.

A bimodal lognormal aerosol module representing the nitrate–ammonium-sulphate–water system is implemented, following Ackermann (1997) and Binkowski and Shankar (1995). This module treats the aerosol number and mass concentration of the different ionic and carbonaceous components in the two lognormal modes, the dispersion being held fixed at present. The physical processes implemented in the aerosol module are coagulation, homogeneous binary nucleation (of H_2SO_4), gaseous condensation/absorption, and dry deposition. Aerosol emissions can also be taken into account whenever data are available. Interaction with cloud droplets is presently not activated, neither is the treatment of sea-salt aerosol particles.

3. Experimental dataset and simulation conditions

During each Lagrangian experiment (Lag1, Lag2, and Lag3 hereafter), three MRF/C130 flights were made. Lag1 and Lag2 were started at midnight, Lag3 began around noon. The flight plan consisted of a stack of horizontal box pattern in and above the MBL with interseeded vertical soundings (Johnson et al., 2000a). Throughout the experiment, the aircraft drifted with the wind and repositioned itself with respect to the "smart" marker balloons, as can be seen in Fig. 1 for Lag2. A total of about eight profiles is available for each Lagrangian experiment, but we limit ourselves here to present mainly comparisons with 1 profile per flight, that is, the initial profile, a profile from the second flight of the Lagrangian experiment, and the last profile from each final flight.

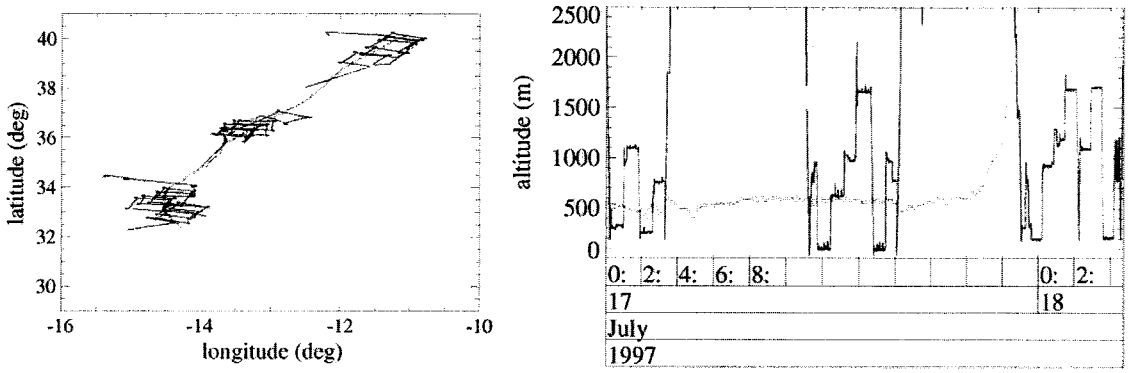

Fig. 1. Position of the MRF/C130 aircraft (thin line) on its three research flights of Lagrangian experiment 2 with respect to the "smart" balloon (crosses/thick line). The three flights may be distinguished by the gaps between the profiles and boxes, the overall direction of the balloon was is the south-west direction.

The original MRF/C130 data was obtained through the ACE-2 data management system in its original high temporal resolution (up to 32 Hz). In order to rearrange this large data set to a convenient shape for modelling purposes, it was first averaged on a 1 Hz timeline. For each vertical profile, the 1 Hz data was then averaged onto a vertical grid with a 50 m resolution. The parameters that were treated in this way and that are presented here are: potential temperature, total water mixing ratio, liquid water mixing ratio, photolysis rates (J_{NO_2}), carbon monoxide (CO), ozone (O_3), and hydrogen peroxide (H_2O_2). Height is expressed using pressure altitude, corrected by the average difference between pressure and radiometric altitude below 500 m. Volatile organic carbon (VOC) measurements were made using a canister sampling system, sulphur dioxide (SO_2) and aerosol chemical composition using filter packs (Andreae et al., 2000). About 10–20 samples are available per Lagrangian experiment for each of these parameters. A detailed description of the different measurement techniques that were used on the MRF/C130 can be found in the ACE-2 data management system (http://ace2.ei.jrc.it.8181/). In this context, it should be noted again that no NO_x measurements were available on the MRF/C130. The only information on these species are available from measurements on Tenerife located near the end of the Lagrangian experiment, where NO_x concentrations were typically of the order of 100 ppb. Therefore, initial NO_x concentrations were varied in the model until the final NO_x concentrations agreed with what was measured at Tenerife.

As already stated earlier, all three Lagrangian experiments took place under anticyclonic, hence subsident conditions in an air mass moving southward over warmer water. In order to represent the effect of this particular meteorological setting, three types of large-scale forcings are introduced in the 1-D model: (1) the sea-surface temperature (SST), (2) the subsidence velocity, and (3) the geostrophic wind. All these parameters are varying as a function of time and position of the simulated air mass. Typically, these forcing terms are extracted from the European Centre for Medium Range Weather Forecast (ECMWF) meteorological analyses [S98]. However, in the case of Lag3, the ECMWF derived subsidence velocity was largely overestimating the observed subsident movement in the free troposphere, indicated by a much too rapid downward advection of the isentropes with respect to observations. For Lag3 we thus decided to use a vertical velocity, deduced from the observed downward movement of the isentropes. Since during all three Lagrangian experiments the wind speed and direction were rather constant in the vertical and the wind shear was weak especially in the MBL (Johnson et al., 2000b; Osborne et al., 2000; Wood et al., 2000), we decided to use a geostrophic wind velocity that is constant with altitude and in time for Lag2 (8 m s^{-1}) and Lag3 (10 m s^{-1}). For Lag1, where wind speeds evolved more largely throughout the experiment, we used a vertically constant wind speed, with varying intensity following the observations (8–12 m s^{-1}). As in S98, the SST was increased by 1 K in the case of Lag2. The reasons for this modification will be discussed below.

4. Results

We will now present the simulation results of all three Lagrangian experiments by direct comparison of aircraft soundings with model profiles. It should be borne in mind that we are here comparing ALL grid points of the model with mostly ALL available observations from the ACE-2 Lagrangian experiments, not only averaged model quantities. Therefore, it is clear that in some cases differences occur between observation and simulation, these differences being particularly exagerrated when gradients are strong.

4.1. Subsidence in the free troposphere

Fig. 2 presents three potential temperature profiles from each of the Lagrangian experiments together with the corresponding model profiles. The effect of subsidence can be identified when looking at the potential temperature change at a given height in the free troposphere or on the vertical displacement of different layers, visible for example in the profiles of total water mixing ratio (Fig. 3), CO (Fig. 6), O_3 (Fig. 7), and H_2O_2 (Fig. 8).

Lag1 is obviously the Lagrangian experiment that is most difficult to be modeled, as can be seen on the potential temperature and total water mixing ratio profiles in the free troposphere. Unfortunately, this is also the Lagrangian with the largest gaps in data coverage. No H_2O_2 measurements were made on the first and third flight of Lag1, and no CO observations are available on the initial profile. Tests regarding the model sensitivity towards its initial conditions (in the case of Lag1) also revealed a large dependance on the choice of the initial temperature and humidity profiles. There was considerable difference between the model runs when replacing the first by the second full aircraft sounding in the initialization.

Generally, in all three cases the model reproduces the observations in the free troposphere, not always with total precision, but the general features are visible. Differences between model and observations may basically have four different reasons (in addition to limitations coming from the parametrizations used in model chemistry and physics). First, there is always some uncertainty in the vertical velocity forcing that is derived from ECMWF-analysed divergence. This could be improved iteratively by modifying the applied subsidence velocity

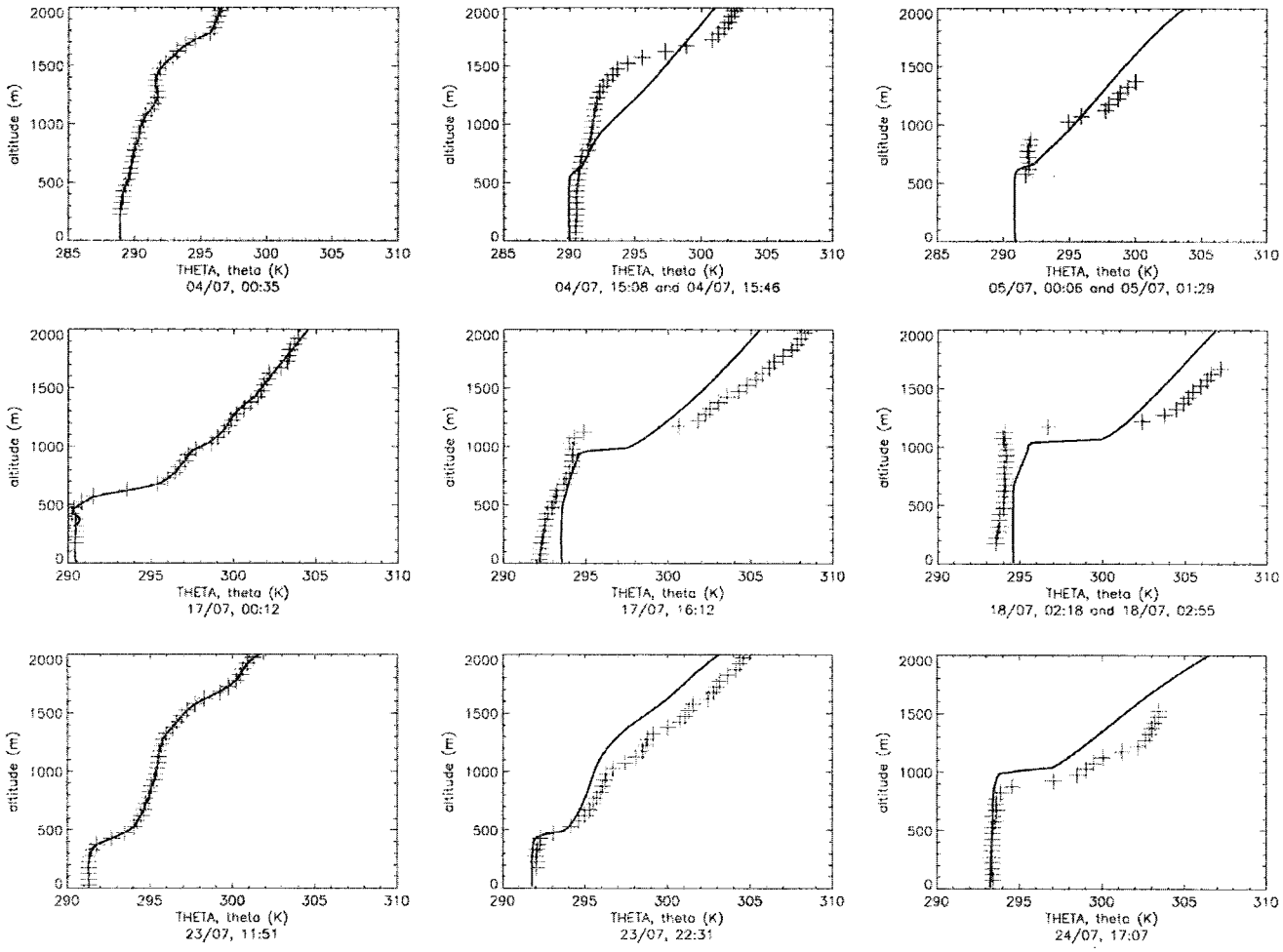

Fig. 2. Observed (crosses) and simulated (solid line) potential temperature for three selected profiles for Lagrangian 1 (top row), for Lagrangian 2 (middle row), and for Lagrangian 3 (bottom row). The profiles in the left column are from the beginning of the first flight in each Lagrangian experiment. They are used for initialization. The profiles in the middle column are from the second flight in each experiment, and the profile in the right column are from the end of each third flight. Time and date of each profile is printed below each graph. In some cases two succesive profiles were collated. Then the time of each subprofile is indicated.

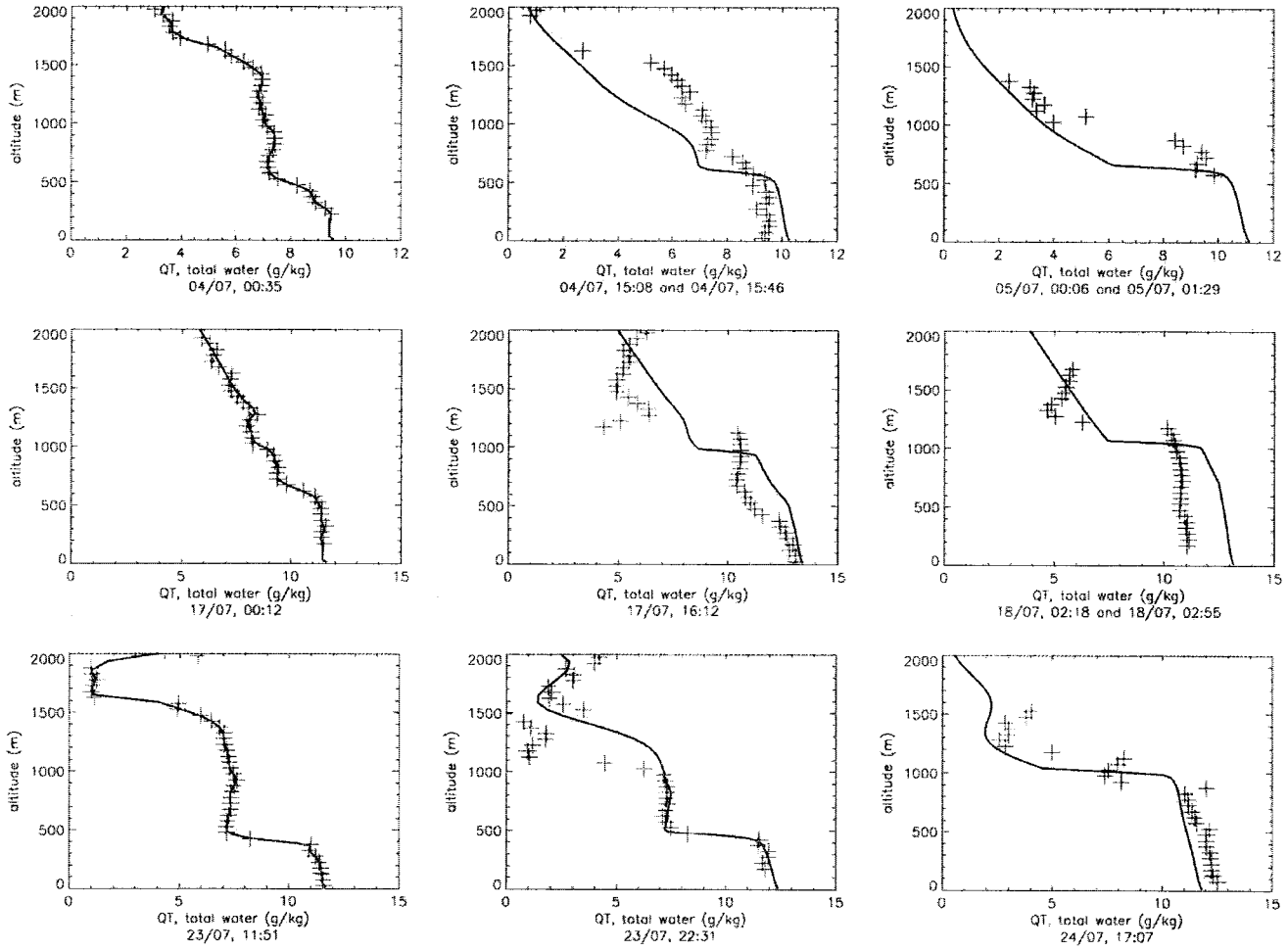

Fig. 3. As in Fig. 2, but for total water-vapor mixing ratio.

forcing, as it has already been done for Lag3. However, it is not our purpose to obtain a total agreement between model and observations by tuning the different model parameters, but to run as far as possible on the basis of objectively constrained parameters, that is, base on ECMWF analyses. Therefore, this is done only for Lag3 where the effect is too important to be ignored.

A second reason for differences between model and observations in the free troposphere for all modelled variables is differential advection. In the presence of vertical wind shear together with horizontal gradients in the observed variables, the Lagrangian concept breaks down since in this case the air mass can no longer be represented as a vertical column. As stated earlier, this effect is minimal in the boundary layer, but becomes more important with altitude. For example, during Lag2 the wind shear between the surface and the inversion was generally less than $3\,\mathrm{m\,s^{-1}\,km^{-1}}$ (Osborne et al., 2000). Introduction of additional forcing terms representing differential advection in the free troposphere could eventually be added, based on further analysis of the observed vertical wind shear, but again, this kind of model tuning is beyond the scope of this paper.

A third reason for differences between the model and the observations in the free troposphere lies in the presence of small-scale heterogeneities. In particular, when the aircraft entered and left the experimental area, it did not fly in spirals, but headed in and out of the experimental zone on a straight line. Whereas in the MBL, turbulence tends to mix horizontal gradients rather quickly, this is not the case in the nonturbulent layers in the free troposphere. Small-scale heterogeneities can be viewed as being the finger prints of the emitter regions, over which air mass passed earlier on its voyage. Those fine-scale structures may have conserved their properties when the turbulence in the RCBL broke down when the air mass moved out over the ocean. Here a slight difference in aircraft position may result in large differences for variables like CO and O_3, especially in the case of the polluted Lagrangians.

Finally, note that with increasing simulation time the influence of the upper boundary conditions become

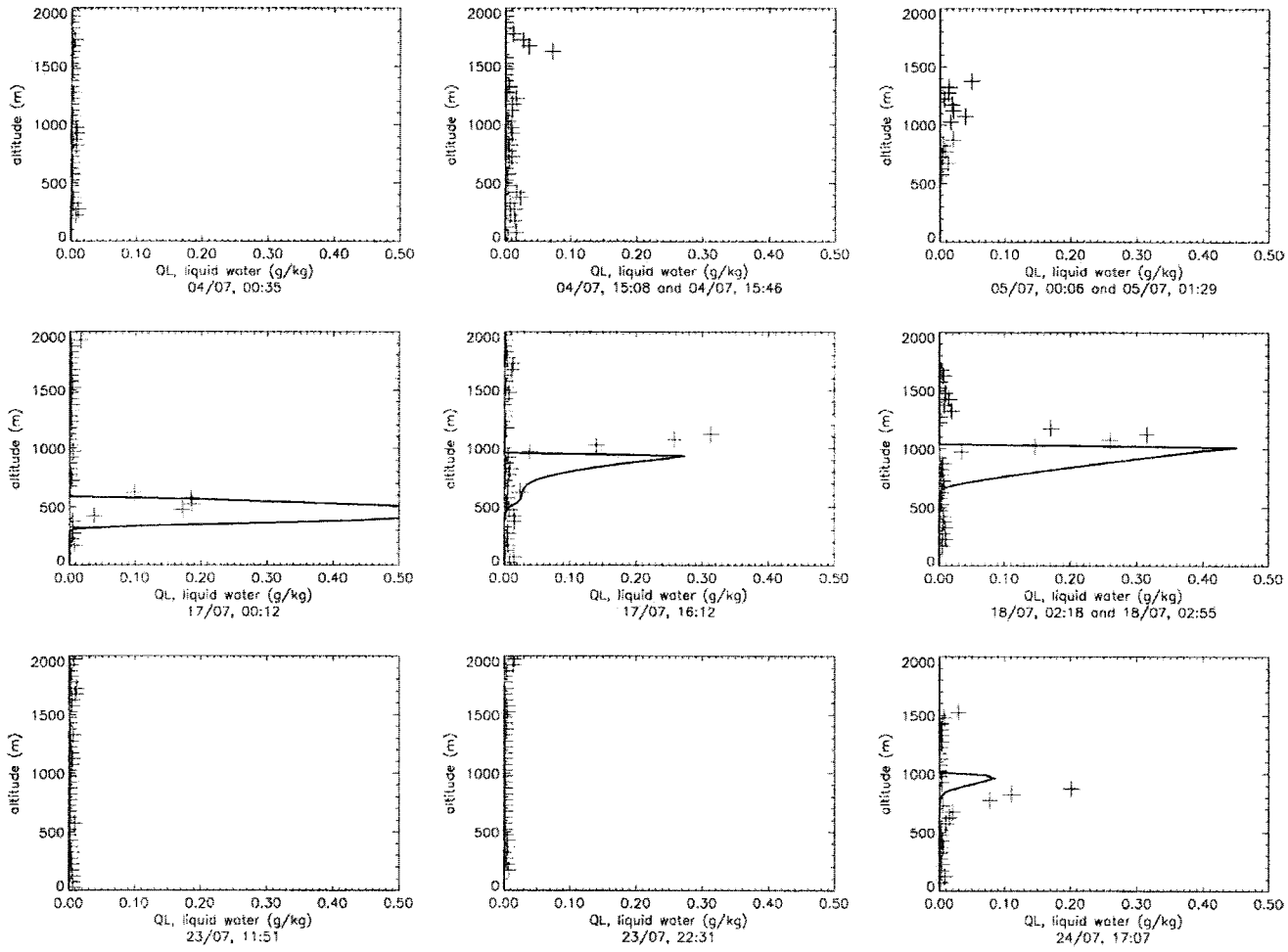

Fig. 4. As in Fig. 2, but for cloud–water mixing ratio.

important. During one day, under the influence of a subsidence velocity of typically $1.2\,\mathrm{cm\,s^{-1}}$, the layers in the free troposphere are advected downward by about 1000 m. This means that the model domain that is above 1800 m is dominated after 24 h of simulation by the upper boundary conditions of the model and not by the initial observational data (the model top is at 2800 m). This effect can be clearly seen in the case of O_3 and CO in Lag2 and Lag3. Theoretically, the model top could be raised, but the effect of differential advection and the increasing distance between the aircraft and the balloon with altitude on the inbound flight would become equally larger. A nudging technique using aircraft data from subsequent flights in altitude could improve this situation. However, for the purpose of modelling the chemistry in the MBL on the time scales we are studying here. this is not important since the domain influenced by the upper boundary conditions remains always above 1500 m altitude, even at the end of the experiment.

4.2. Boundary layer growth and entrainment

The development of a deepening MBL as the air mass moves over warmer water can be clearly seen in the cases of Lag2 and Lag3, where considerable boundary layer growth occurred. Note that in the case of Lag2 we had to increase the sea-surface temperature by about 1 K with respect to the ECMWF analysis to compensate for a too weak boundary layer development with respect to the observations. Such a difference is within the uncertainty in the ECMWF SST analysis (S98). The effect of entrainment, which is the cumulated effect of subsidence and boundary layer growth, can be most clearly seen on the ozone profiles of Lag2 and the CO profiles of Lag3. In both cases, a pollutant-rich residual continental boundary layer overlaid the MBL in the beginning of the experiment.

Carbon monoxide can be regarded as a passive tracer on the time scale of the ACE-2 Lagrangian experiments. Therefore, it allows the verification of vertical transport

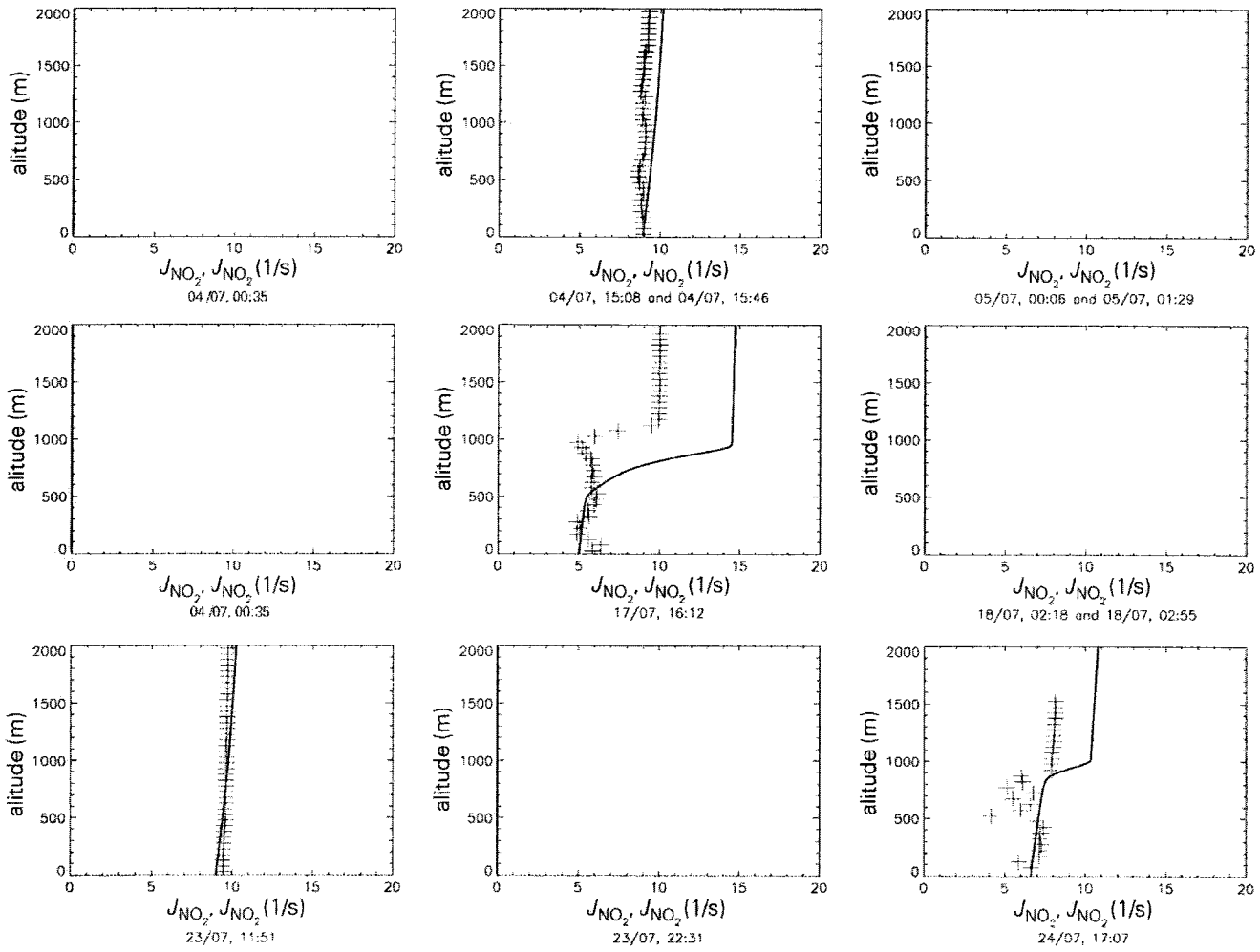

Fig. 5. As in Fig. 2, but for photolysis rates (J_{NO_2}).

processes in the absence of chemical reactions. As can be seen in Fig. 6, the model is able to reproduce the CO vertical structure rather correctly. As for the Lag1 experiment, the wind speed was higher in the cloud layer than in the MBL and there was often wind shear through the transition layer and the subsidence inversion (Johnson et al., 2000b). As a consequence, since the presence of vertical shear above the MBL weakens the 1D Lagrangian hypothesis, the CO simulation does not accurately reproduce the RCBL evolution. Carbon monoxide modelling provides good results for the two polluted Lagrangian experiments, in particular the erosion of the polluted RCBL in Lag3 by boundary layer growth from below and its squeezing by subsidence from above.

Ozone mixing ratio in the MBL of Lag2 increase from initially 35 ppb to about 50 ppb in the end due to entrainment of the RCBL air with an O_3 mixing ratio of 65 ppb (Fig. 7). This process is quite well reproduced by the model. In Lag3, in contrast, the model also tends to increase O_3 in the MBL due to entrainment, but here the observed O_3 mixing ratio remains low, leading to a difference of about 10 ppb between model and observations by the end of the experiment. If we look at the corresponding H_2O_2 profiles we note that the model also overestimates the H_2O_2 production in the MBL quite largely for this experiment. As we know from the CO simulations, entrainment of a chemically passive species should be correctly reproduced by the model. This suggests then that in Lag3, in contrast to Lag2, ozone photochemistry is not entirely captured by the model. A probable reason for this may be the uncertainty in the estimate of NO_x concentrations, that unfortunately, were not made on board of the MRF/C130. Further sensitivity studies with the model might shed more light on this question, but they are also speculative and are therefore not included in this paper.

4.3. *Photochemistry*

There are a number of parameters of the meteorological model, apart from subsidence and vertical transport, that impact the photochemical simulations: The

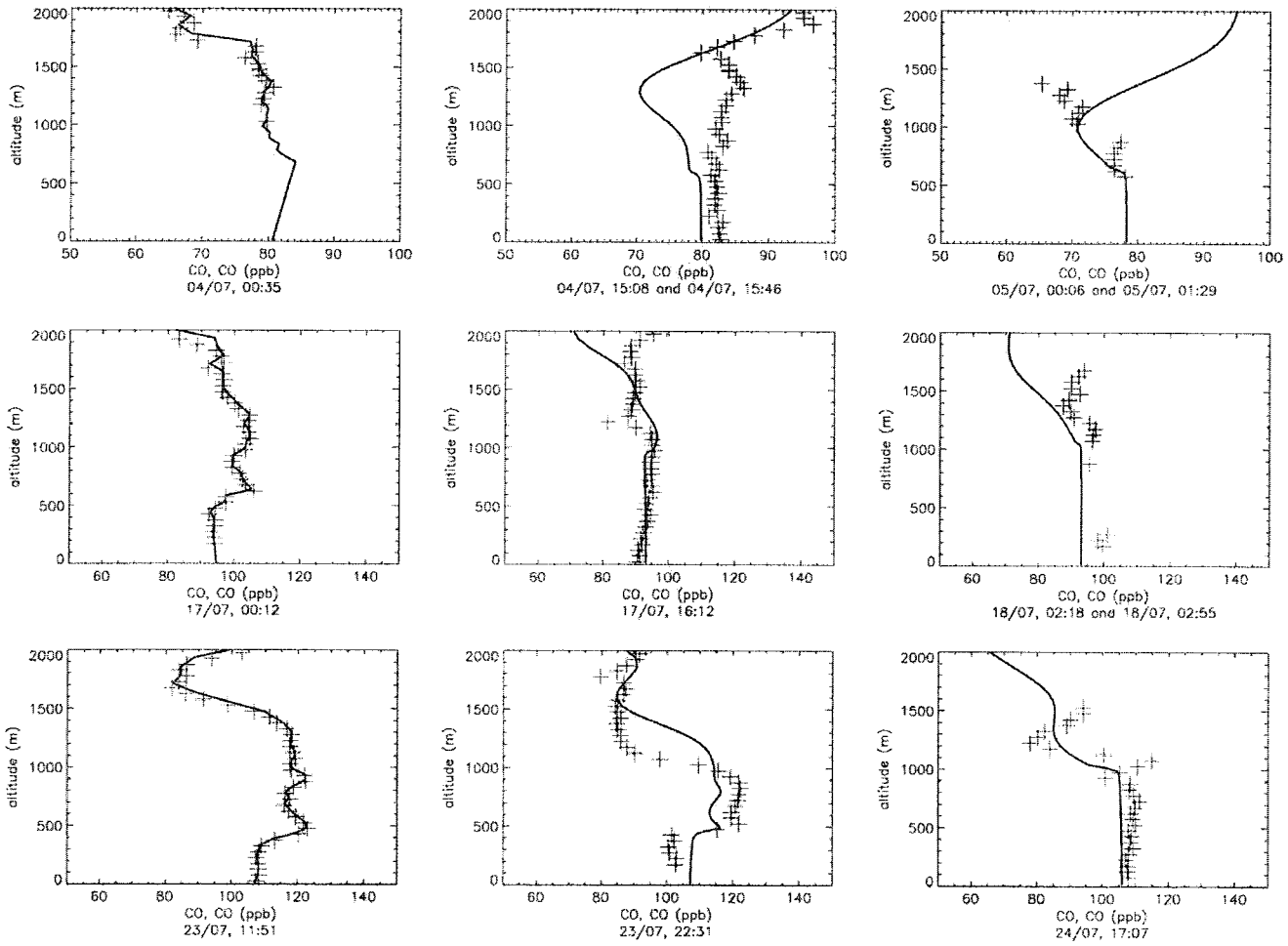

Fig. 6. As in Fig. 2, but for CO mixing ratio.

aerodynamic resistance at the surface, which is a function of modelled surface wind speed and stability in the surface layer, is used in the calculation of the dry deposition velocities (Seinfeld and Pandis, 1998 and references therein). The modelled cloud–water profile intervenes in the calculation of the photolysis rates as well as in the liquid-phase chemistry part of the model. Reaction constants are temperature dependent, and water vapor is an important reactant in the $O(^1D) + H_2O$ reaction, where it is responsible for ozone loss and OH production. The effect of dry deposition can be clearly seen on the hydrogen peroxide profiles in the MBL (Fig. 8), whereas the effect of clouds on the photolysis rates J_{NO_2} is visible in particular in Figs. 4 and 5 on the second profile of Lag2 and the third profile of Lag3. The presence of clouds results in both cases in an enhancement of the actinic flux above the cloud, due to the much higher albedo of the cloud with respect to that of the ocean. The model agrees qualitatively, but overestimates this effect in the case of Lag2. This is probably due to a modelled cloud water profile that differs somewhat from the observations, and further to the fact that the modelled cloud optical properties are related by a simple semiempirical relationship to the cloud liquid water content (Fouquart, 1987), assuming in particular horizontally homogeneous clouds. Under clear sky conditions, in contrast, the modelled J_{NO_2} values are in excellent agreement with the observations.

As stated earlier, the RACM reaction mechanism (Stockwell et al., 1997) with 77 species and 237 reactions was used in this simulation. As this is a condensed mechanism, several volatile organic carbon (VOC) species are lumped in one model species as a function of their reactivity. Fig. 9 presents an example for model species HC3, which is the sum of the observed species *n*-butane, isobutane, acetylene, and cyclopropane. As can be seen from this figure, during all three Lagrangian experiments, mixing ratios of these species were relatively low in comparison with polluted continental episodes. The same statement holds for the higher organic compounds, so that none of the three experiments can be considered to represent a highly VOC-polluted case. In addition, the

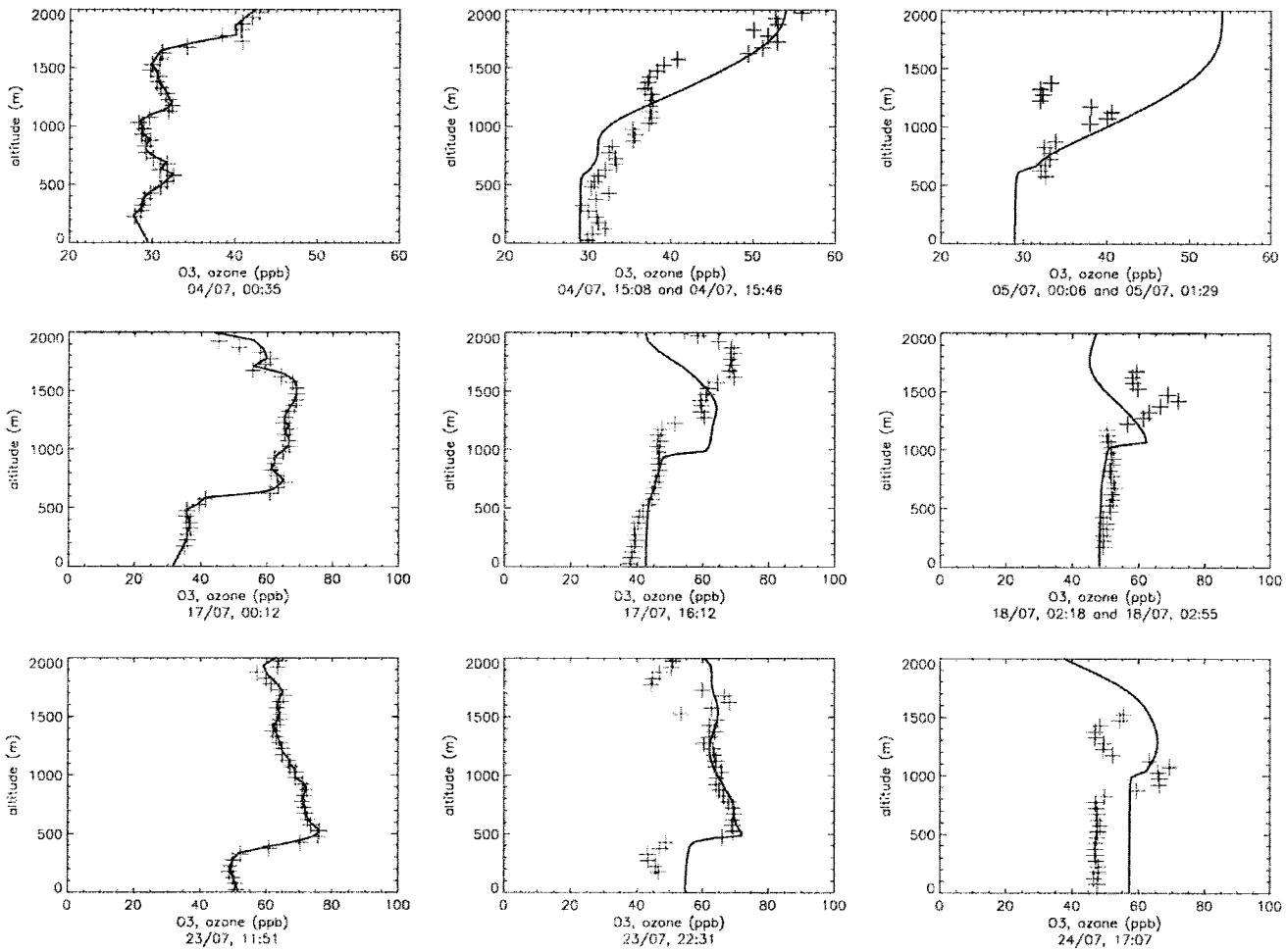

Fig. 7. As in Fig. 2, but for O_3 mixing ratio.

low number of VOC observations per Lagrangian experiments makes it difficult to initialize those variables on a vertical profile. Here we use vertically constant mixing ratio. As can be seen from Fig. 9, the model is able to represent both the destruction and mixing of HC3 during daytime and this with about the correct amplitude (except maybe for Lag1 where VOC concentrations were particularly low and hence the signal-to-noise ratio relatively high). However, one should notice that, given its relatively important lifetime, destruction is not the most important diurnal evolution process of HC3.

4.4. Cloud chemistry

Lag2 had the largest amount of cloud cover of all three Lagrangians. It was overcast throughout the experiment. However, as shown by (Suhre et al., submitted), cloud formation had only just onset when the Lagrangian experiment started. This gave a unique opportunity to observe the in-cloud oxidation of SO_2 by H_2O_2, which as shown below was completed in a time span of less than 4 h. The air mass that was sampled during Lag2 has left the Iberian peninsula about 12 h earlier, after passing over a region where substantial sources of SO_2 (power plants) are located. The effect of H_2O_2 removal from the MBL between the sounding at 0012 UTC and 0323 UTC is quite visible in Fig. 10, both on the observed and modelled profiles. When the initially relatively high SO_2 amount of 800 ppt is consumed, H_2O_2 concentrations increase again (Fig. 11), still exhibiting a vertical profile with a minimum near the surface due to its high dry deposition velocity. This evolution is well reproduced by the model.

Fig. 11 shows a scatterplot of observed SO_2 and H_2O_2 which shows the strong anticorrelation between both species, except for one point in the free troposphere, where no in-cloud oxidation takes place. The same behaviour can be seen on the scatterplot of the model variables: a cloud of points representing the free troposphere, the initial decrease of both species (arrows) due to aqueous-phase oxidation, followed by a continued decrease of SO_2 and an increase in H_2O_2 due to its

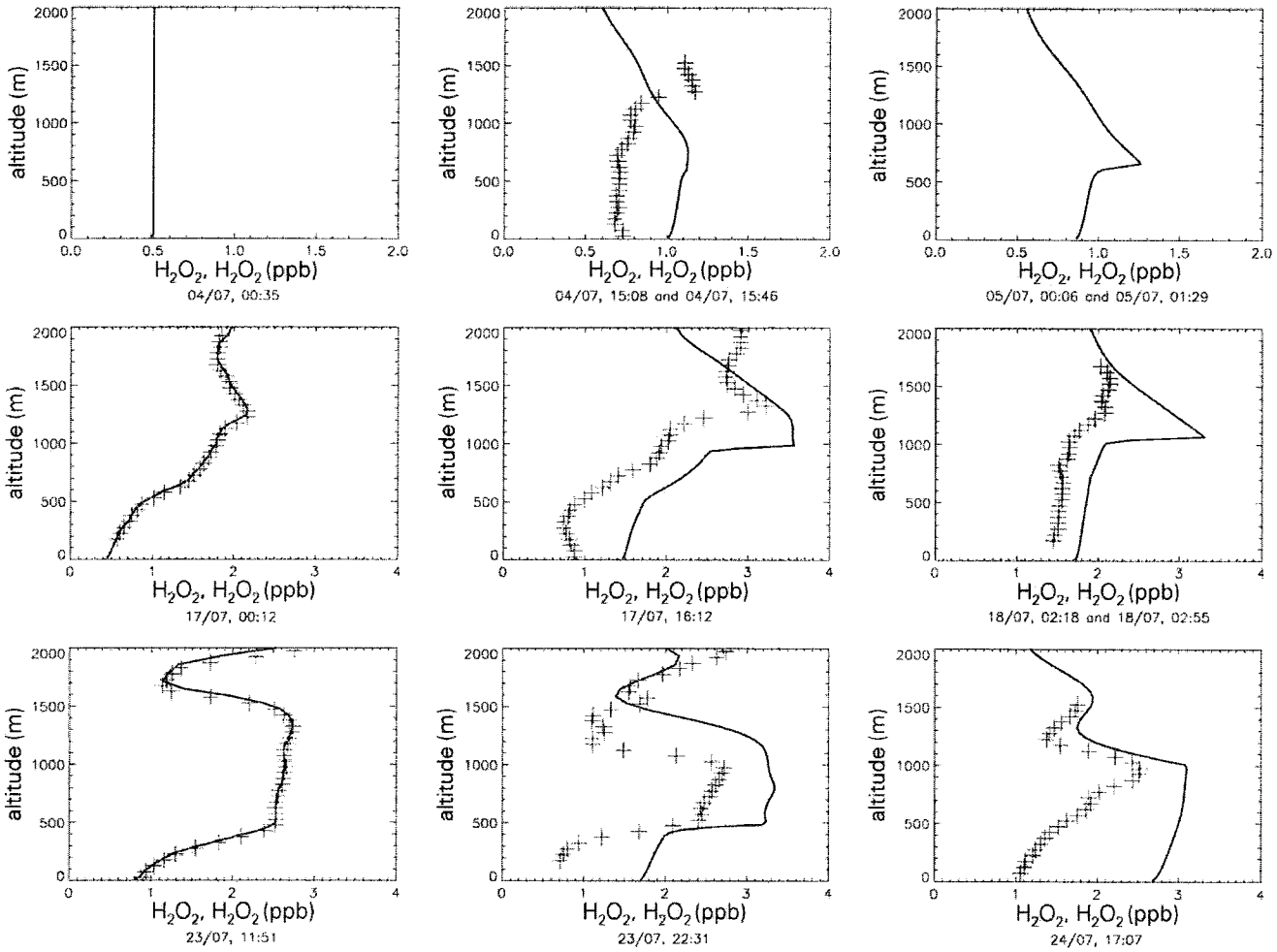

Fig. 8. As in Fig. 2, but for H_2O_2 mixing ratio.

gas-phase production and mixing. What is also interesting to note is the line of dots that links the free tropospheric values with the low-SO_2/ high-H_2O_2 dots. These are due to the entrainment of free tropospheric air into the MBL later in the experiment. Due to rapid replenishment of H_2O_2 both by turbulent mixing in the MBL and by gaseous phase production, SO_2 concentrations decrease rapidly after entrainment into the MBL by in-cloud oxidation and mixing, but H_2O_2 concentrations barely change.

4.5. Preliminary results from the aerosol module

Finally, a comparison between a time-scale analysis (Hoell et al., 2000) and a bimodal lognormal aerosol chemistry module is performed. This detailed time-scale analysis is based upon measured data and includes processes such as coagulation, condensation, deposition, chemical processing, sea-salt flux and entrainment. As a consequence, since sea-salt treatment and aerosol cycling in model clouds have not yet been taken into account, the following results are still preliminary.

The initial aerosol distribution in the model was obtained by fitting two lognormal modes to the aerosol size distributions from Hoell et al. (2000). This constrains for each mode the total aerosol number and mass concentration, as well as the dispersion of the lognormal distributions. In practice, the key parameters in this iterative initialization process is in fact not the total aerosol mass, but the sulphate mass in each mode, since sulphate is the only species that is considered as being nonvolatile by the aerosol equilibrium model (Ackermann, 1997; Binkowski and Shankar, 1995). For NO_3 and NH_3, their total concentrations in the gas and in the aerosol phase are treated prognostically. The model then determines at each timestep what fraction of these species actually enters the aerosol phase for each mode. The total ionic mass for aerosol particles smaller than 1.5 μm (Andreae et al., 2000) is used to determine the total NH_3 and NO_3 concentrations. The observed total SO_4 mass is first

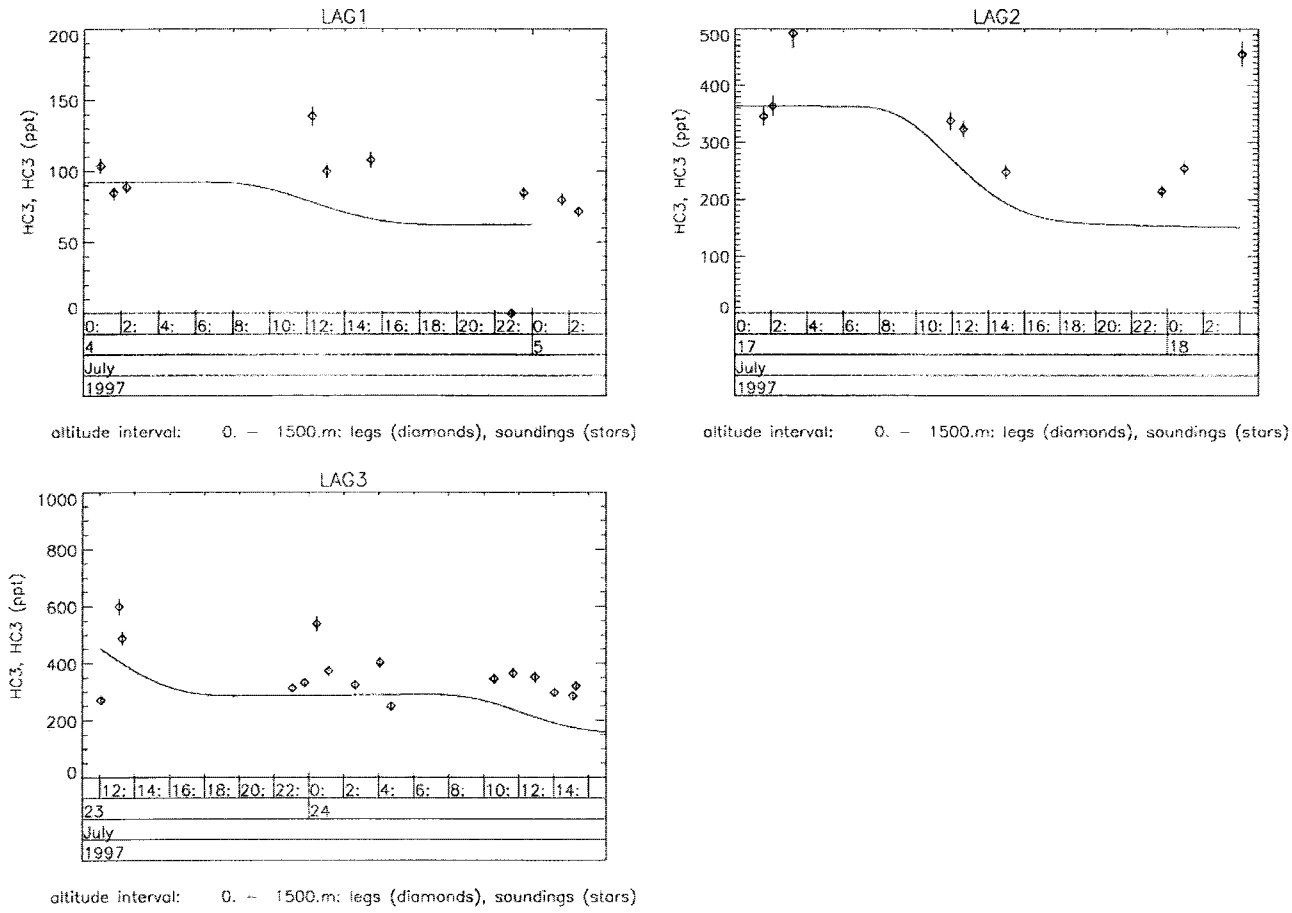

Fig. 9. HC3 organics time series for Lagrangian 1 (top left), 2 (top right), and 3 (bottom). Observations below 1500 m are plotted as dots and the model average over the 0–1500 m range is presented as the solid lines.

distributed onto the small mode (which is in fact only a small fraction of the total mass), and the remaining SO_4 is then attributed to the large mode. In the case of Lag1 and Lag3 it turns out that this mass is not sufficient to make up for the total aerosol mass that is needed to obtain the aerosol number distribution from Hoell et al. (2000). This missing mass (which is in fact the difference between the ionic mass from the filter samples and the total mass from the optical counters) is then associated to the larger mode as a chemically passive, unspecified species. Some of this difference may be due to sampling losses in the inlet system (Andreae et al., 2000). Also, we presently do not account for NaCl (sea-salt) aerosols, which clearly dominated the larger of the two modes (Hoell et al., 2000) in Lag1. Putaud et al. (private communication) have shown that the larger aerosol particles may also contain an important amount of organic matter, which would not show up in the ionic analysis.

Fig. 12 shows the aerosol number distribution in the MBL as derived by Hoell et al. (2000). Their time-scale analysis points out that the enhancement of the larger mode is mainly due to sea-salt aerosol flux into the reduced mixed layer volume: since no sea-salt emissions are taken into account in our aerosol module, modelling does not simulate any change in the larger mode (however, for the Lag2 experiment, the larger mode was mainly controlled by entrainment, which was correctly reproduced by the aerosol module). Moreover, Hoell et al. (2000) show that the finer mode is controlled by coagulation and condensation processes of what is basically a ammonium–sulphate aerosol. Our aerosol module properly describes the impact of these processes so that, as can be seen in Fig. 12, the model correctly accounts for a decrease in aerosol number in the fine mode (similar results were obtained for the fine mode in Lag2: Lag3 was not treated by Hoell et al.). Parallel to the decrease in aerosol number, modelling shows that the fine mode mean diameter increases accordingly. However, this change in the fine mode diameter does not appear in measured data. Indeed, one should note that no direct observations of the aerosol number distribution are available on the MRF/C130 for size cuts below

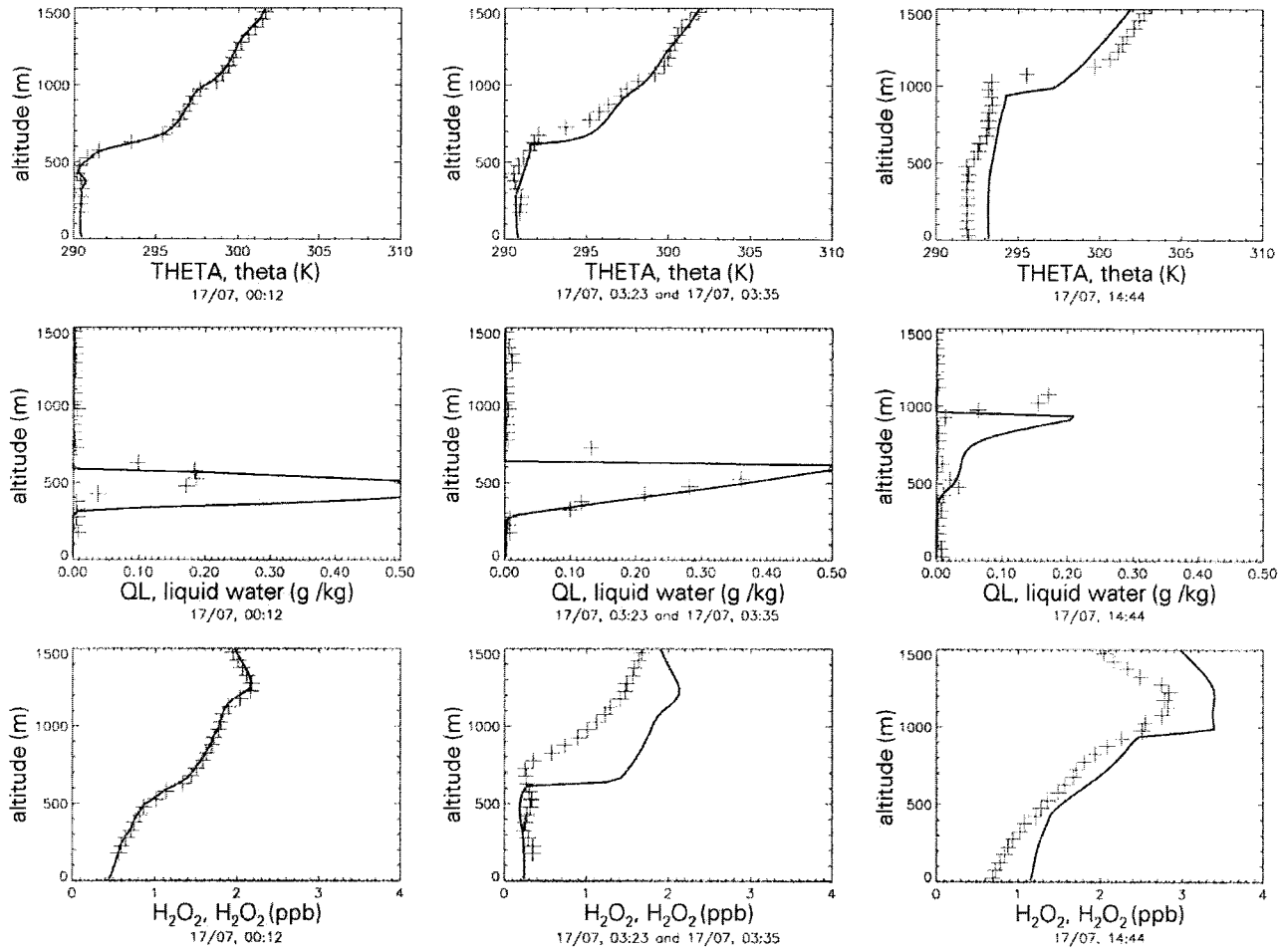

Fig. 10. Observed (crosses) and simulated (solid line) of potential temperature (top row), cloud–water mixing ratio (middle row), and H_2O_2 mixing ratio (bottom row) for Lagrangian experiment 2. Presented are the initial profiles (left column) at 0012 UTC, at 0330 UTC (middle row), and at 1444 UTC (right row).

0.1 μm. To obtain the aerosol spectra presented in Fig. 12, Hoell et al. (2000) used the aerosol spectrum observed on the research vessel R/V *Vodyanitsky* at the start of the Lagrangian experiments and scaled it with the total number of nucleating particles (CN) observed on the aircraft. Therefore, the shape of the spectrum below 0.1 μm does not change in those graphs, as in reality it should have, and as it does in fact in the simulation.

In order to give an idea of the vertical distribution of the water mass associated with the aerosol, Fig. 13 shows a profile of the aerosol composition in the fine mode at the end of Lag1. It can be seen that most changes in aerosol mass is due to different amounts of water uptake. Note that the initial vertical profile of all aerosol parameters was assumed to be vertically constant (SO_4 mixing ratio, total NH_3 and NO_3 mass, total aerosol number mixing ratio, mean mode diameter), which represents a rather strong assumption, and which may be relaxed in the futur by further analysis of the aerosol measurements made on board of the MRF/C130. It is clear that this part, which is the most interesting with respect to aerosol radiative forcing questions, still requires much development, like for example the introduction of a sea-salt mode to the model and parameterization of aerosol cycling in the model clouds. Validation would eventually be possible using for instance aerosol optical thickness measurements that are also available in ACE-2.

5. Conclusion

The dynamical and chemical evolution of the three ACE-2 Lagrangian experiments was modelled, accounting for boundary layer meteorogical processes such as turbulence, cloud formation and entrainment, and chemical processes in the gas, cloud and aerosol phase. By direct comparison of simulated profiles and aircraft

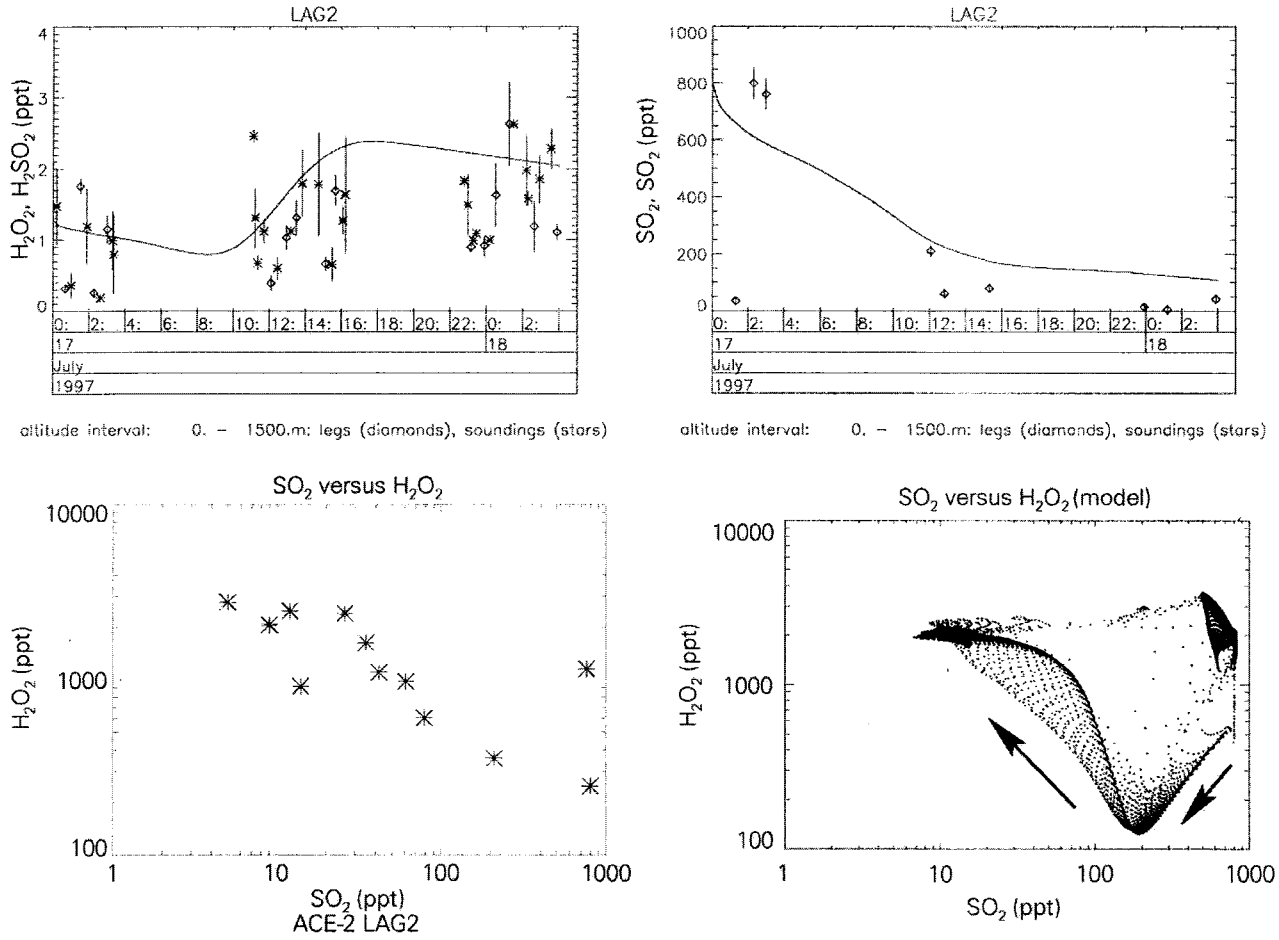

Fig. 11. Hydrogen peroxide (top left) and SO_2 (top right) time series for Lagrangian 2. Observations below 1500 m are plotted as dots and the model average over 0–1500 m range is presented as the solid lines. Sulphur dioxide and H_2O_2 crossplot, observations (bottom left) and modelled (bottom right). Observed H_2O_2 mixing ratios are averaged over the sampling time of the SO_2 filter pack. Model results are presented for all grid points recorded at a 10 min interval.

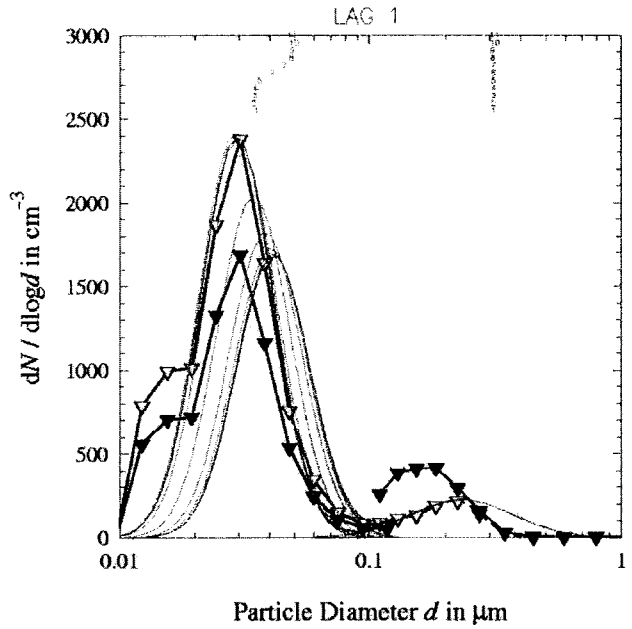

soundings of temperature, humidity cloud-water content, O_3, CO, and H_2O_2 over periods of more than 24 h different aspects of the model's ability to represent the observed system were analysed.

We show that the model is able to represent the dynamical evolution of the marine boundary layer, in one case requiring adjustment of the subsidence velocity (Lagrangian 3) and the surface heat fluxes (Lagrangian 2). Sensitivity to the initial conditions is greater in the case of Lagrangian 1, where interchanging the first aircraft sounding by the second in the initialization leads to

Fig. 12. Aerosol number distribution adapted from Hoell et al. (2000) for the Lagrangian experiment 1. Open (full) triangles correspond to a spectrum in the MBL at the start (end) of the experiment. The modelled aerosol number distribution at 100 m altitude is presented equally spaced in time by the different solid lines. Peak aerosol number decreases in time and the mean mode diameter increases.

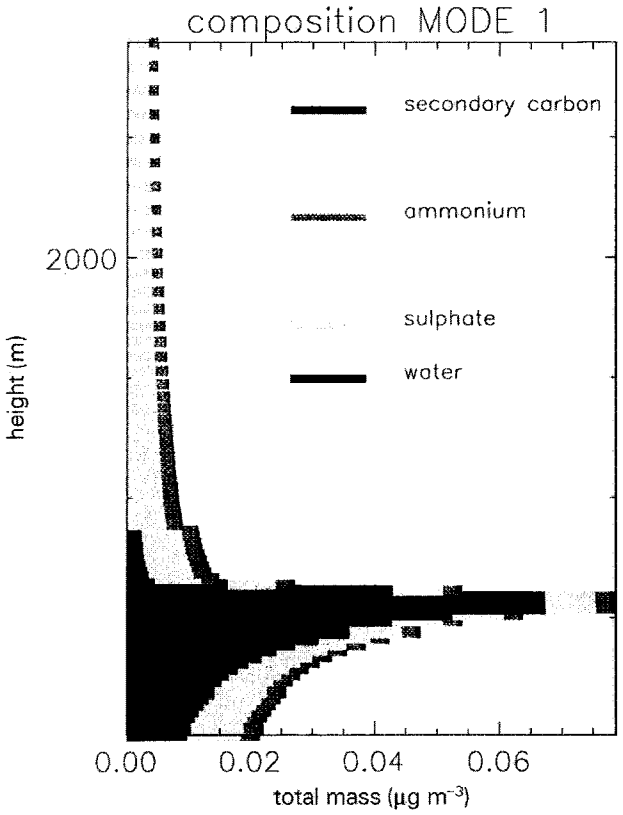

Fig. 13. Vertical profile of the aerosol composition of the small mode at the end of Lagrangian experiment 1. Each horizontal line corresponds to one model level.

considerably different results in the boundary layer evolution.

Entrainment of a layer rich in ozone (Lagrangian 2) and CO (Lagrangian 3) from the residual continental boundary layer into the marine boundary layer is simulated by the model. However, lack of NO_x measurements limits our ability to constrain the chemical simulation sufficiently to determine the reasons for a disagreement between ozone and H_2O_2 simulations and observations in the case of Lagrangian 3.

Probably, the most satisfying result from this study is the simulation of the in-cloud oxidation of SO_2 by H_2O_2 in the case of Lagrangian 2, where the model is able to reproduce the evolution of the H_2O_2 profile in the boundary layer as well as the observed anti-correlation between both species to a good degree of agreement.

Finally, preliminary results of a simulation with a bimodal aerosol chemistry module are presented. In order to simulated the ACE-2 Lagrangian experiments completely, introduction of a sea-salt mode as well as parameterization of aerosol cycling in clouds still needs to be introduced into the model. However, coherent results are obtained for the small, presumably SO_4–NH_3 aerosol mode, which is dominated by coagulation and condensational growth processes.

Acknowledgements

This research is a contribution to the International Global Atmospheric Chemistry (IGAC). Core project of the International Geosphere–Biosphere Programme (IGBP) and is part of the IGAC Aerosol Characterization Experiments (ACE). Financial support has been allocated by the national research programme on atmospheric chemistry (PNCA). We thank P. Bechtold, P. Mascart, J. P. Pinty, and E. Richard for many helpful discussions, and M. Louge for the contributions she made through her Masters thesis work. Analysed meteorological data was made available by the European Centre for Medium Range Weather Forecast (ECMWF). The development of the Méso-NH model is supported by CNRS/INSU.

References

Ackermann, I.J., 1997. MADE: Entwicklung und Anwendung eines Aerosol-Dynamikmodells für dreidimensionale Chemie-Transport-Simulationen in der Troposphäre. In: A. Ebel, M. Kerschgens, F.M. Neubauer, and P. Speth, Köln (Eds.). Mitteilungen aus dem Institut für Geophysik und Meteorologie der Universität Köln.

Andreae, M.O., Elbert, W., Gabriel, R., Johnson, D.W., Osborne, S., Wood, R., 2000. Soluble ion chemistry of the atmospheric aerosol and SO_2 concentrations over the eastern North Atlantic during ACE-2. Tellus B, in press.

Bechtold, P., Fravalo, C., Pinty, J.P., 1992. A model of marine boundary layer cloudiness for mesoscale applications. Journal of Atmospheric Science 49, 1723–1744.

Binkowski, F.S., Shankar, U., 1995. The regional particulate model 1. Model description and preliminary results. Journal of Geophysical Research 100, 26191–26209.

Bougeault, P., Lacarrère, P., 1989. Parameterization of orography-induced turbulence in a meso-beta model. Monthly Weather Review 117, 1872–1890.

Bretherton, C.S., Pincus, R., 1995. Cloudiness and marine boundary layer dynamics in the ASTEX Lagrangian experiments. 1. Synoptic setting and vertical structure. Journal of Atmospheric Science 52, 2707–2723.

Businger, S., Chiswell, S.R., Ulmer, W.C., Johnson, R., 1996. Balloons as a Lagrangian measurement platform for atmospheric research. Journal of Geophysical Research 101, 4363–4376.

Businger, S., Johnson, R., Katzfey, J., Siems, S., Wang, Q., 1999. Smart tetroons for Lagrangian air-mass tracking during ACE 1. Journal of Geophysical Research 104, 11709–11722.

Charnock, H., 1955. Wind stress on a water surface. Quarternary Journal of Royal Meteorological Society 81, 639.

Fouquart, Y., 1987. Radiative transfer in climate modelling. In: M.E. Schlesinger (Ed.), NATO Advanced Study Institute on Physically-Based Modeling and Simulation of Climate and Climatic Changes. 223–283.

Hoell, C., O'Dowd, C., Osborne, S., Johnson, D.W., 2000. Timescale analysis of marine boundary layer aerosol evolution: Lagrangian case studies under clean and polluted cloudy conditions. Tellus B (52B), 423–438.

Huebert, B.J., Pszenny, A.A., Blomquist, B., 1996. The ASTEX/MAGE Experiment. Journal of Geophysical Research 101, 4319–4329.

Johnson, D.W., Osborne, S., Wood, R., Suhre, K., Johnson, R., Businger, S., Quinn, P.K., Wiedensohler, A., Durkee, P.A., Russell, L.M., Andreae, M.O., O'Dowd C., Noone, K., Bandy, B., Rudolph, J., Rapsomanikis, S., 2000a. An overview of the Lagrangian experiments undertaken during the North Atlantic regional aerosol characterization experiment (ACE-2). Tellus B, in press.

Johnson, D.W., Osborne, S., Wood, R., Suhre, K., Quinn, P.K., Bates, T.S., Andreae, M.O., Noone, K., Glantz, P., Bandy, B., Rudolph, J., O'Dowd, C., 2000b. Observations of the evolution of the aerosol, cloud and boundary layer characteristics during the first ACE 2 Lagrangian experiment. Tellus B, in press.

Kessler, E., 1969. On the distribution and continuity of water substance in atmospheric circulations. Meteorological Monographs 10 (32), 84.

Lafore, J.P., Stein, J., Asencio, N., Bougeault, P., Ducrocq, V., Duron, J., Fischer, C., Héreil, P., Mascart, P., Pinty, J.P., Redelsperger, J.L., Richard, E., Vilá-Guerau de Arellano, J., 1998. The Meso-NH atmospheric simulation system, I, adiabatic formulation and control simulations. Annals of Geophysics 16, 90–109.

Madronich, S., Flocke, S., 1998. The role of solar radiation in atmospheric chemistry. In: Boule, P. (Ed.), Handbook of Environmental Chemistry. Springer, Heidelberg, pp. 1–26.

Morcrette, J.-J., 1989. Impact of changes of the radiation transfer parameterizations plus cloud optical properties in the ECMWF model. Monthly Weather Review 118, 847–873.

Morcrette, J.-J., Fouquart, Y., 1985. On systematic errors in parametrized calculations of longwave radiation transfer. Quarterly Journal of the Royal Meteorological Society 111, 691–708.

Osborne, S.R., Johnson, D.W., Wood, R., Bandy, B.J., Andreae, M.O., O'Dowd, C.D., Glantz, P., Noone, K., Rudolph, J., Bates, T., Quinn, P., 2000. Evolution of the aerosol, cloud and boundary layer dynamic and thermodynamic characteristics during the second Lagrangian experiment of ACE-2. Tellus B, in press.

Raes, F., 1995. Entrainment of free tropospheric aerosols as a regulating mechanism for cloud condensation nuclei in the remote marine boundary layer. Journal of Geophysical Research 100, 2893–2903.

Raes, F., Bates, T.S., McGovern, F., Vanliedekerke, M., 2000. The second aerosol characterization experiment (ACE-2): overview. Tellus B, in press.

Redelsperger, J.L., Sommeria, G., 1981. Méthode de représentation de la turbulence d'échelle inférieure à la maille pour un modéle tri-dimensionnel de convection nuageuse. Boundary Layer Meteorology 21, 509–530.

Russel, L.M., Lenshow, D.H., Laursen, K.K., Krummel, P.B., Siems, S.T., Bandy, A.R., Thornton, D.C., Bates, T.S., 1998. Bidirectional mixing in an ACE 1 marine boundary layer over-lain by a second turbulent layer. Journal of Geophysical Research 103, 16411–16432.

Seinfeld, J.H., Pandis, S.N., 1998. Atmospheric Chemistry and Physics. From Air Pollution to Climate Change. Wiley, New York.

Stockwell, R.W., Kirchner, F., Kuhn, M., Seefeld, S., 1997. A new mechanism for regional atmospheric chemistry modeling. Journal of Geophysical Research 102, 25847–25879.

Stull, R.B., 1988. An Introduction to Boundary Layer Meteorology. Kluwer Academic Publishers, Norwell.

Suhre, K., Andreae, M.O., Rosset, R., 1995. Biogenic sulfur emissions and aerosols over tropical South Atlantic II. One-dimensional simulation of sulfur chemistry in the marine boundary layer. Journal of Geophysical Research 100 (D6), 11323–11334.

Suhre, K., Johnson, D.W., Rosset, R., Osborne, S., Wood, R., Bates, T.S., Raes, F., 2000. A continental outbreak of air that occurred during the Second Aerosol Characterization Experiment (ACE 2): Mesoscale modelling of Lagrangian experiment 2. Journal of Geophysical Research, submitted for publication.

Suhre, K., Mari, C., Bates, T.S., Johnson, J.E., Rosset, R., Wang, Q., Bandy, A., Blake, D., Businger, S., Eisele, F.L., Huebert, B.J., Kok, G., Mauldin III, R.L., Prévôt, A.S.H., Schillawski, R., Thornton, D., 1998. Physico-chemical modeling of ACE 1 Lagrangian B. 1. a moving column approach. Journal of Geophysical Research 103, 16433–16456.

Suhre, K., Rosset, R., 1994. DMS oxidation and turbulent transport in the marine boundary layer: a numerical study. Journal of Atmospheric Chemistry 18, 379–395.

Van Dop, H., Addis, R., Fraser, G., Girardi, F., Graziani, G., Inoue, Y., Kelly, N., Klug, W., Kulmala, A., Nodop, K., Pretel, J., 1998. ETEX: A European tracer experiment; observations, dispersion modelling and emergency response. Atmospheric Environment 32, 4089–4094.

Wang, Q., Lenschow, D.H., Pan, L., Schillawski, R.D., Kok, G.L., Laursen, K., Russell, L.M., Bandy, A., Thornton, D., Suhre, K., 2000. Characteristics of the marine boundary layer during Lagrangian measurements, Part II: Turbulence structure. Journal of Geophysical Research 104, 21767–21784.

Wood, R., Johnson, D.W., Osborne, S., Andreae, M.O., Bandy, B., Bates, T.S., O'Dowd, C., Glantz, P., Noone, K., Quinn, P.K., Rudolph, J., Suhre, K., 2000. Boundary layer and aerosol evolution during the third Lagrangian experiment of ACE 2. Tellus B (52B), 401–422.